The Effect of Water on the Adsorption of NO_2 in Na− and Ba−Y, FAU Zeolites: A Combined FTIR and TPD Investigation

János Szanyi,* Ja Hun Kwak, and Charles H. F. Peden

Chemical Sciences Division, Pacific Northwest National Laboratory, P.O. Box 999, MSIN K8−93, Richland, Washington 99352

Received: November 13, 2003; In Final Form: January 16, 2004

The adsorption of NO_2 was investigated and compared on Na− and Ba−Y, FAU zeolites both in the absence and presence of adsorbed water using FTIR and TPD techniques. The same ionic NO_x species (NO^+, NO^+-NO_2, NO_3^-), formed by the disproportionation of NO_2, were observed to form on both materials under dry conditions at room temperature. The thermal stabilities of these species, however, were vastly different on the two materials. Room-temperature evacuation was sufficient to decompose the NO^+NO_2 adduct in Na−Y, while this species was stable up to 350K over Ba−Y. The adsorbed NO^+ was also much more stable over Ba−Y than on Na−Y. Water significantly affected the adsorbed NO_x species on both materials. In the presence of water, the IR signatures of adsorbed NO^+ were eliminated from both catalysts; however, it did not affect the IR feature of the NO^+NO_2 species on Ba−Y. In the TPD spectra, the NO_2 desorption peak shifted from 350 K to 520 K on Na−Y preexposed to water. In Ba−Y, the high-temperature NO_2 desorption feature of ∼470 K shifted to ∼620 K as a result of adsorption on the water-containing sample, while the low-temperature peak remained unchanged.

Introduction

The removal of NO_x from automotive exhaust gases is a tremendous challenge to the catalytic community, in particular when the engine is operated under lean conditions, that is, in excess oxygen (e.g., diesel engines). Under these conditions, the traditional three-way catalysts do not work because of their very high activity for hydrocarbon oxidation that results in the depletion of the reducing agent before NO_x reduction can take place. Therefore, several emerging technologies are being considered for diesel exhaust aftertreatment. Among the most promising ones are the NO_x adsorber[1] and the nonthermal plasma assisted catalytic NO_x reduction technologies.[2−13] Base metal oxide adsorbers (in particular BaO) are highly effective for the removal of NO_x from an oxygen-rich exhaust gas mixture. Recently, we reported very promising activities for both Na− and Ba−Y, FAU zeolites in the catalytic lean NO_x reduction, when the catalyst was used in conjunction with a nonthermal plasma.[14] In the plasma, reactive species are formed that are converted to benign compounds over these base catalysts. The two most important reactions that take place in the plasma are the almost complete conversion of NO to NO_2 and the formation of partially oxidized hydrocarbon species (e.g., acetaldehyde) in significant quantities. Combining the strong oxidizing power of NO_2 and the ease of oxidizeability of CH_3-CHO results in high level of NO_x reduction over these base zeolite catalysts at relatively low temperatures (∼473 K).

In our previous work,[15] we reported that exchanging the charge-compensating Na^+ ions for Ba^{2+} ions in Y, FAU (Y) zeolites increases the NO_x conversion by more than 10% and also widens the temperature window in which high activity can be sustained. We have suggested that one possible explanation of this activity enhancement was the stronger adsorption of NO_2 observed over Ba−Y in comparison to Na−Y. Here, we report on our recent finding on the adsorption of NO_2 on both Na− and Ba−Y. We used FTIR spectroscopy to identify the nature of adsorbed species and correlated those finding with the results obtained from the temperature-programmed desorption (TPD) of NO_2. The adsorption and desorption of NO_2 were investigated on both water-free (dry) and water-containing (wet) catalysts. The results show significant differences between the Na− and Ba−Y zeolites in NO_2 adsorption. The possible consequences of these findings on their catalytic activities will also be discussed.

Experimental Section

The catalyst materials used in this study were prepared from a Na−Y zeolite obtained from Zeolyst International (CBV 100) and had a Si/Al ratio of 2.5. For the studies on Na−Y, the commercial powder material was used without any modification. The preparation of the Ba−Y catalysts used in this study was identical to the Ba−Y (2−2) material used in our previous study.[14] Briefly, the starting Na−Y zeolite was ion exchanged twice with aqueous Ba−acetate solutions at 353 K, then washed with deionized water. After each ion-exchange step, the catalyst was dried at room temperature and then calcined in air at 773 K for 4 h to reach a high ion exchange level. XRD showed that both the starting Na−Y and the prepared Ba−Y were highly crystalline. ^{27}Al and ^{29}Si NMR were used to verify the absence of extraframework aluminum.

The FTIR measurements were carried out with a Mattson Research Series FTIR spectrometer, equipped with an MCT detector, and operated at 4 cm^{-1} resolution. Each spectrum was an average of 256 scans. The IR cell was a stainless steel six-way cube attached to both a pumping and a gas handling station and equipped with CaF_2 windows. The base pressure of the cell was less than 1×10^{-6}Torr, and the maximum pressure attainable was 1000 Torr. The powder zeolite sample was

* Corresponding author. E-mail: janos.szanyi@pnl.gov.

10.1021/jp037472v CCC: $27.50
Published on Web 03/02/2004

pressed onto a fine-tungsten mesh, which in turn was attached to copper heating legs sitting on ceramic feed-throughs. This setup allows the resistive heating of the sample to ~1000 K and cooling to ~100 K. The sample temperature was monitored through a chromel/alumel thermocouple spot welded to the top center of the tungsten grid.

After the sample was mounted in the IR cell, it was gradually heated to 773 K in a vacuum and kept at that temperature for at least 2 h to ensure the removal of water from the zeolite pores. (We also commonly baked the IR cell and the gas manifold during dehydration to minimize the readsorption of water from the walls of the IR cell into the zeolite upon completion of the annealing.) Adsorption experiments on the thus prepared samples were conducted in the following fashion: In the NO_2 adsorption experiments, NO_2 aliquots in increasing amounts were added to the sample. After 5 min equilibration time, an IR spectrum was acquired after each gas introduction. Upon completion of the adsorption experiment, the stability of the adsorbed NO_x species were examined by first evacuating the sample at room temperature and then gradually heating it up to higher temperature ($T_{max.} = 773$ K). In the experiment when the effect of H_2O on the NO_2 adsorption was studied, first a given amount of water was added to the catalyst followed by the step-by-step addition of NO_2. These experiments were also carried out in a reverse order of adsorption, that is, the sample was first saturated with NO_2 and then H_2O was added in increasing amounts.

The NO_2 adsorption and TPD experiments were conducted on an RXM 100 catalyst characterization system (ASDI). The catalyst (~0.025 gr) was placed into a quartz reactor, evacuated at room temperature, and then annealed at 773 K for 2 h (the base pressure in the reactor after catalyst activation was $<2 \times 10^{-7}$Torr). NO_2 then was adsorbed on the dehydrated catalyst. The reactor was evacuated until the base pressure dropped below 1×10^{-6} Torr and then a TPD program was run from 293 to 773 K at a heating rate of 5 K/min. The masses were monitored by a UTI 100 mass spectrometer, and the intensities of a series of masses were recorded. The masses monitored were 18 (H_2O), 28 (N_2 or CO), 30 (NO), 32 (O_2), 44 (N_2O or CO_2) and 46 (NO_2). In the TPD spectra discussed in the following section, we show only the spectra for mass 30, since this was the most intense fragmentation species of NO_2. Mass 46 (NO_2) and mass 30 (NO) always followed the same desorption pattern in these TPD experiments.

Results and Discussion

The adsorption of NO_2 on Na−Y has been discussed in detail in our previous publication.[16] We have shown that upon NO_2 adsorption, NO^+ and NO_3^- species are formed as a result of the well-known disproportionation of NO_2 that takes place on solid catalyst surfaces[16]

$$2NO_2 \leftrightarrow NO^+ + NO_3^- \quad (1)$$

The formed NO^+ binds to an O^- site of the zeolite framework, replacing a charge-compensating Na^+ ion, while the NO_3^- binds to a Na^+ ion. In the presence of excess NO_2, adsorption complexes such as NO^+NO_2 or $NO^+N_2O_4$ can form as well. A series of IR spectra of the NO_2 adsorption on Na−Y is displayed in panel A of Figure 1 as a function of the amount of NO_2 dosed. At low NO_2 doses, a doublet feature is seen in the 1350−1450 cm^{-1} range and a band at 2017 cm^{-1}. The 1350−1450 cm^{-1} doublet represents the split ν_3 vibrations of adsorbed NO_3^-.[17] The 2017 cm^{-1} band belongs to the N−O stretching

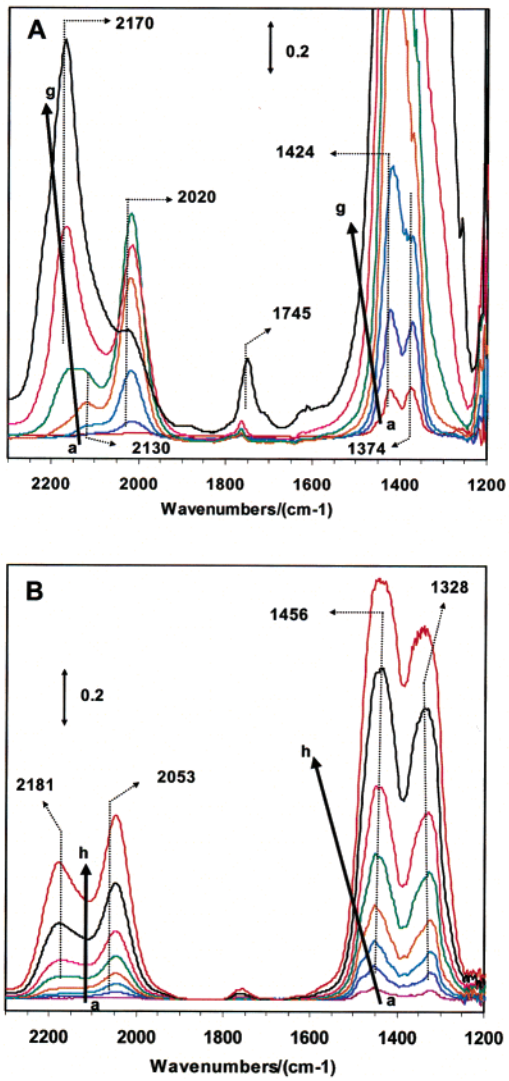

Figure 1. FTIR spectra following NO_2 adsorption on Na− (A) and Ba−Y (B) at 295 K. NO_2 doses (μmol): A: 2.13 (a), 5.74 (b), 13.6 (c), 28.5 (d), 56.7 (e), 123 (f), 258 (g); B: 0.465 (a), 1.46 (b), 2.91 (c), 5.08 (d), 7.83 (e), 11.7 (f), 19.9 (g), and 32.1 (h).

vibration of the adsorbed NO^+ species.[17] A shoulder on the high-frequency side of this feature may indicate NO^+ adsorption on different sites available inside the zeolite structure. With increasing NO_2 doses, the intensities of the IR features representing both NO_3^- and NO^+ increase, and a new IR feature starts developing at 2170 cm^{-1} at higher NO_2 doses. We have assigned this high-frequency absorption band to a NO^+NO_2 type of adsorption complex. As this feature develops, the intensity of the band representing NO^+ decreases.

There is a second mechanism for the adsorption of NO_2 on zeolites that involves water that is almost always present in the zeolite structure even after the most careful dehydration procedure. In this process, HNO_3 is formed that can readily initiate the

$$-O^-....Na^+ + HNO_3 \leftrightarrow -O^-...H^+ + NaNO_3^- \quad (2)$$

ion exchange. The thus formed Brønsted acidic site represents new adsorption centers for NO_2. The NO^+ species formed upon the interaction of NO_2 with these protonic sites are represented by the IR feature at 2160 cm^{-1} (the same IR band is seen when H−Y is contacted with NO_2).

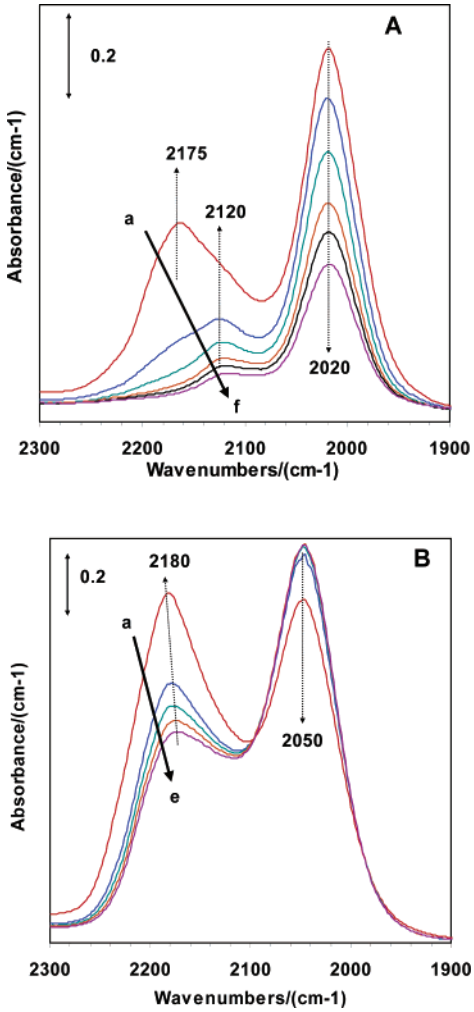

Figure 2. FTIR spectra after evacuation at 295 K following NO_2 adsorption on Na− (A) and Ba−Y. Evacuation time (min): A: 1 (a), 5 (b), 10 (c), 20 (d), 40 (e), 60 (f); B: 0 (a), 5 (b), 10 (c), 30 (d), and 65 (e).

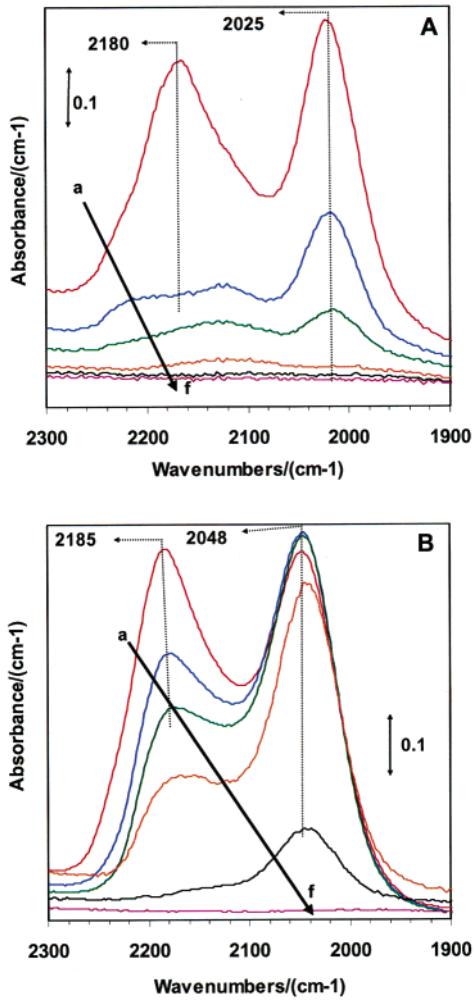

Figure 3. The effect of annealing on the FTRIR spectra after NO_2 adsorption on Na− (A) and Ba−Y (B). A: in the presence of 0.2 Torr NO_2 (a), after 16-min evacuation at 295 K (b), annealing for 1 min at 373 K (c), 473 K (d), 573 K (e), and 673 K (f); B: in the presence of 0.2 Torr NO_2 (a), after 30-min evacuation at 295 K (b), annealing at 373 K (c), 473 K (d), 573 K (e), and 673 K (f).

The IR features that arise upon the adsorption of NO_2 on Ba−Y are shown in panel B of Figure 1 as a function of the amount of NO_2 dosed. Comparison of the absorption bands in panel A and B of Figure 1 reveals that the adsorbed species are very similar on both Na− and Ba−Y zeolites. At low NO_2 doses, we observe the nitrate (1300−1500 cm^{-1}) and NO^+ (2053 cm^{-1}) species adsorbed onto Ba−Y. With increasing amount of NO_2 introduced onto the sample, the intensities of these bands increase gradually; furthermore, new IR features develop at the high frequence side of the 2053 cm^{-1} band. After the saturation of the 2053 cm^{-1} feature, an intense band develops at 2180 cm^{-1} (similarly to the 2170 cm^{-1} band over Na−Y). We assign this feature to a NO^+NO_2 type of adduct.

The adsorption of NO_x on zeolites has been studied extensively by FTIR spectroscopy and the results of these investigations were summarized in a recent review article by Hadjiivanov.[17] In most of the zeolite materials studied, several adsorbed ionic species were observed upon the adsorption of NO_2 and in the reaction of NO + O_2 as well. Today it is commonly accepted that because of the disproportionation reaction of NO_2, NO^+ and NO_3^- species are formed inside the zeolites and are strongly held through ionic interactions. Above a threshold NO_2 pressure, NO^+ can form NO^+NO_2 or $NO^+N_2O_4$ adducts. In most cases, these adducts, however, are very unstable, and can easily lose NO_2 to reconvert to NO^+.

The stabilities of the adsorbed NO_x species of Na− and Ba−Y at room temperature under vacuum can be deduced from the IR spectra shown in Figure 2, panels A and B, respectively. Under these conditions, the IR band representing the NO^+NO_2 adduct (2170 cm^{-1}) on the NO_2-saturated Na−Y is almost completely removed by a 1-min evacuation suggesting that this species is very unstable in the absence of gas-phase NO_2 on this sample. Even the intensity of the 2020 cm^{-1} band (adsorbed NO^+) is markedly decreased upon room-temperature evacuation. On Ba−Y, however, both the NO^+ and NO^+NO_2 species are much more stable against room-temperature evacuation than on Na−Y. Although some intensity of the 2180 cm^{-1} band is lost, the 2050 cm^{-1} band remains essentially unchanged. Annealing the NO_2-saturated samples results in the complete removal of the NO^+ adsorbed species at 373 K from Na−Y, while on the Ba−Y sample the intensities of the NO^+NO_2 and NO^+ IR bands gradually decrease (Figure 3). First, the 2180 cm^{-1} feature loses its intensity followed by the decrease in the intensity of the 2050 cm^{-1} band. The NO^+ related IR band (2050 cm^{-1}) possesses some intensity even after annealing at 573 K.

The differences in the thermal stabilities of the adsorbed NO_x species in these two catalysts are well demonstrated by the results of the NO_2 TPD experiments shown in Figure 4 A (Na−Y) and B (Ba−Y). In Na−Y, one desorption feature was

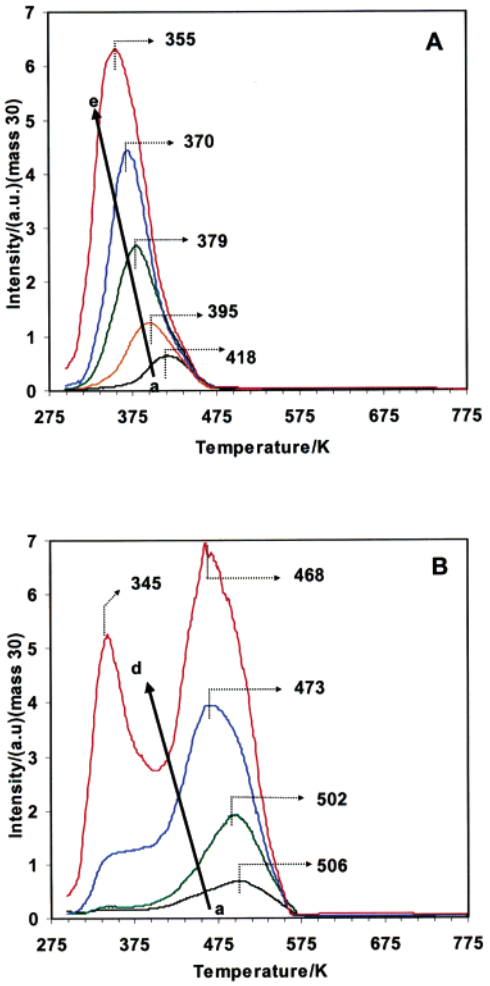

Figure 4. TPD spectra following NO_2 adsorption at 295 K on Na−(A) and Ba−Y (B). NO_2 doses (mmol): A: 2.27 (a), 4.53 (b), 9.07 (c), 13.6 (d), 22.7 (e); B: 4.53 (a), 9.07 (b), 22.7 (c), and 45.3 (d). (Weight of catalyst: 0.025 g; heating rate: 5 K/min.)

observed, and its peak position shifted to lower temperatures as the amount of adsorbed NO_2 was increased. At the lowest NO_2 dose studied, the desorption peak maximum can be seen at 418 K shifting to 355 K at the highest NO_2 dose. In the Ba−Y zeolite, on the other hand, two NO_2 desorption features can be seen (panel B of Figure 4). At the lowest NO_2 dose studied, only one desorption feature is present and its peak position is at 505 K. Increasing the amount of NO_2 adsorbed results in the development of a low-temperature desorption feature, whose peak desorption temperature does not seem to change with increasing amount of NO_2 dosed; it is constant at 345 K. The peak of the high-temperature desorption feature gradually downshifts as the amount of NO_2 adsorbed increases (similarly to the desorption feature of Na−Y). At the highest NO_2 dose studied, the maximum of the high-temperature feature is observed at 468 K. The coverage dependences of both the single NO_2 desorption feature of Na−Y and the high-temperature desorption feature of Ba−Y seem to indicate second-order desorption kinetics. From the desorption peak positions, we can estimate approximate heat of desorption values of 21−25 kcal/mol for Na−Y and 27−30 kcal/mol for Ba−Y. These estimated values may not be representative of the true desorption energies; however, their difference of ∼5−6 kcal/mol is a good indicator of the stronger NO_2 adsorption on Ba−Y than on Na−Y.

The assignments of the TPD features can be made by comparing the results of the TPD with those of the FTIR. After NO_2 adsorption and full evacuation at room temperature, only NO^+ and NO_3^- species are present on the Na−Y sample as shown by the single IR feature present at 2020 cm^{-1} (NO^+) and peaks in the range of 1354−1450 cm^{-1} (NO_3^-). In the TPD experiment, a NO_2 desorption feature (352−418 K) is observed as NO^+ and NO_3^- recombines to give $2NO_2$ molecules and the original clean Na−Y is restored. The situation over Ba−Y is different. After saturation with NO_2 and room-temperature evacuation, we observe two distinct IR absorption features (2048 and 2180 cm^{-1}) because of the high stability of both the NO^+ and the NO^+NO_2 adduct. Therefore, in the TPD experiment we observe two desorption features as well. The low-temperature peak represents the desorption of NO_2 from the NO^+NO_2 adduct, while the high-temperature one arises from the recombination of the NO^+ and NO_3^- species similarly to what we have shown for the NO_2 desorption on Na−Y. The low-temperature NO_2 TPD feature of Na−Y is absent because of the low thermal stability of the NO^+NO_2 adduct on this catalyst.

As we have mentioned in the previous paragraphs, there is more then one mechanistic possibility for NO_2 to adsorb on the Na− and Ba−Y zeolites studied here. One is the disproportionation of NO_2 to form NO^+ and NO_3^- according to reaction **1** that we observe to be operative on the fully dehydrated zeolite samples. The other one is the interaction of NO_2 with adsorbed water in the channels of zeolites. Reactions that may take place between NO_2 and H_2O in the zeolite channels are

$$3NO_2 + H_2O \leftrightarrow 2HNO_3 + NO \quad (3)$$

$$2NO_2 + H_2O \leftrightarrow HNO_3 + HONO \quad (4)$$

The HNO_3 formed in these processes can instantly interact with the charge-compensating ions (Na^+ or Ba^{2+}) creating Brønsted acidic sites and Na(Ba)-nitrates (reaction 2). If this reaction sequence is correct, we expect to see the formation of Brønsted acidic OH groups, Na(Ba)-nitrates, HONO, and no adsorbed NO^+ following NO_2 exposure to hydrated samples. As it turn out, this is exactly the case. Addition of H_2O to a dry Na−Y zeolite results in the appearance of absorption features in the IR spectrum that are characteristic of the adsorbed water in zeolites. The absorption bands represent δ_{HOH} vibrations (1640 cm^{-1}), ν_{OH} vibrations of free O−H groups (3695 cm^{-1}), and ν_{OH} vibrations of associated OH groups (3100−3600 cm^{-1}) of adsorbed water. The broad bands in the 3100−3600 cm^{-1} region arises from water adsorbed onto cations located in different crystallographic positions.[18] A series of IR spectra obtained upon the adsorption of NO_2 on the wet Na−Y zeolite is presented in Figure 5. In this experiment, first water was added to the dry Na−Y, and then NO_2 was introduced onto the wet sample in increasing amounts at room temperature, and changes in the IR spectra were monitored. In Figure 5, spectrum **a** represents a typical IR spectrum of water adsorbed on Na−Y. Addition of a small amount of NO_2 onto the wet Na−Y sample resulted in the appearance of a doublet absorption band that is characteristic of NO_3^- groups associated with Na^+ ions. At the same time, the intensities of both the 3695 cm^{-1} and 1640 cm^{-1} bands of adsorbed water started to decrease. Concomitantly, in the O−H stretching vibrational region new bands appear with peak positions characteristic of Brønsted acidic OH groups of Y zeolites (3640 and 3550 cm^{-1}). The intensities of adsorbed water-related bands gradually decrease, while those of the NO_3^- and zeolitic OH features increase with increasing amounts of NO_2 dosed. With the increase of adsorbed NO_2 amount, a new band develops at the low-frequency side of the NO_3^- bands at 1270

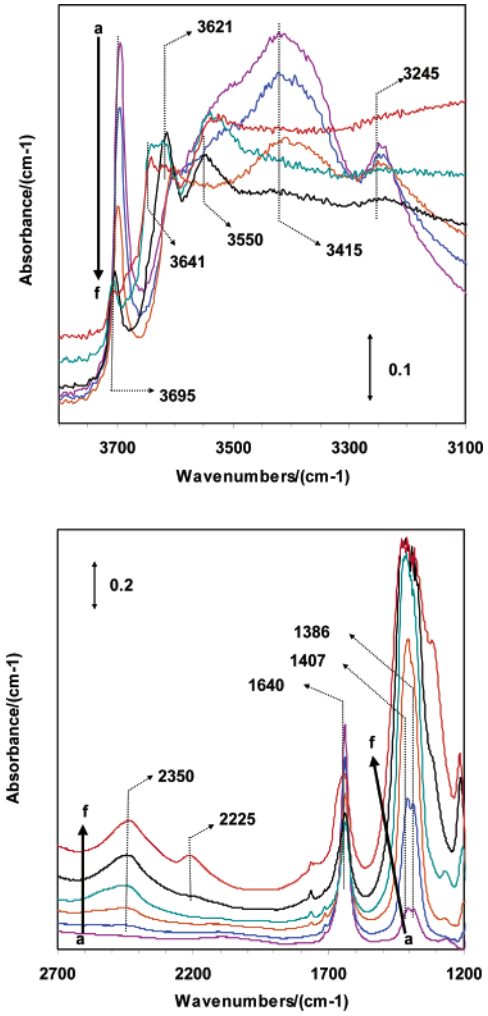

Figure 5. FTIR spectra of NO_2 adsorption on $[H_2O]_{ads}$-Na−Y at 295 K. Doses (μmol): H_2O: 11.1 (a), N_2O: 2.55 (b), 6.98 (c), 17.5 (d), 40.2 (e), and 86.5 (f).

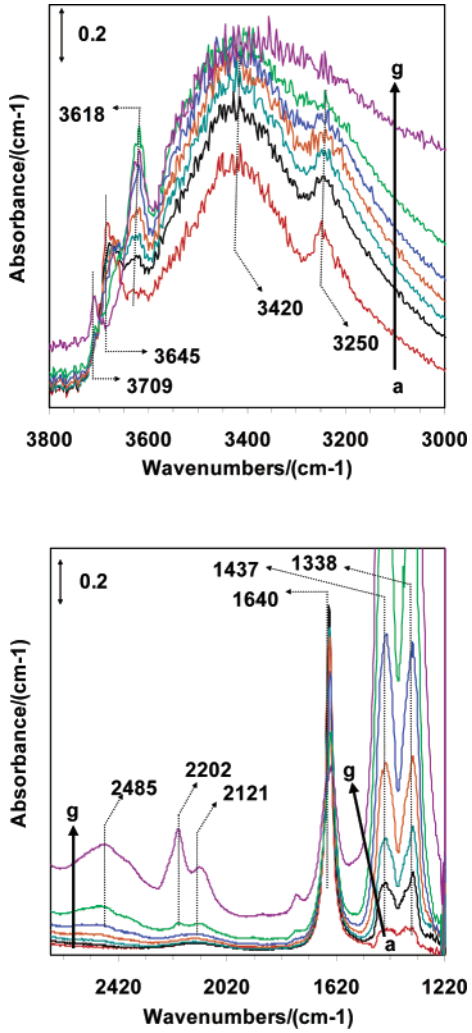

Figure 6. FTIR spectra of NO_2 adsorption on $[H_2O]_{ads}$-Ba−Y at 295 K. Doses (μmol): H_2O: 16.6 (a), NO_2: 2.91 (b), 5.48 (c), 9.55 (d), 17.8 (e), 32.8 (f), and 112 (g).

cm^{-1}. This band represents adsorbed NO_2^- species probably originating from the adsorption of HONO. (This adsorbed surface species is absent when NO_2 is adsorbed onto dry Na−Y.) In the ν_{OH} region, the intensity of the band representing the stronger Brønsted acid sites of Y zeolite at 3640 cm^{-1} decreases after significant amount of NO_2 is added to the system, and a new feature develops at around 3620 cm^{-1}. This ν_{OH} vibration may represent the O−H stretching vibrations of HNO_x molecules formed after all the charge-compensating Na^+ ions were replaced by H^+.

The adsorption of NO_2 on water-exposed Ba−Y follows similar trends to that observed for Na−Y. The series of IR spectra recorded upon the adsorption of NO_2 on wet Ba−Y is displayed in Figure 6. Upon H_2O adsorption on the dry Ba−Y, the δ_{HOH} and ν_{OH} vibrations of adsorbed water are seen at 1640 cm^{-1} and in the 3000−3750 cm^{-1} region, respectively. The addition of a small amount NO_2 results in the appearance of the split nitrate band in the 1300−1500 cm^{-1} range and the development of a new ν_{OH} band at 3620 cm^{-1}. In contrast to the NO_2 adsorption on dry Ba−Y, no IR features of adsorbed NO^+ are seen at low NO_2 pressures. With increasing NO_2 doses, the intensities of the nitrate features increase while that of the adsorbed water decrease. At high NO_2 pressures (in the presence of gas-phase NO_2 in the IR cell), bands representing NO^+ and NO^+NO_2 are visible. It is possible that these latter species are formed on the adsorption sites that were not occupied by water because of the initial low water dose used in the experiment or on the protonic sites of the zeolite. However, it is evident that on both Na− and Ba−Y the presence of water definitely inhibits the formation of NO^+ species, while NO_3^- and NO_2^- species are readily formed. Since there is a competition between NO_2 and H_2O for the same adsorption sites[19] (charge-compensating cations), at small NO_2 doses NO_2 cannot directly interact with the Na^+ or Ba^{2+} ions but rather with the H_2O molecules strongly adsorbed onto these cations. At higher NO_2 pressures, because of the adsorption/desorption equilibrium between H_2O and NO_2, some H_2O-free adsorption sites can open up where NO_2 can adsorb as NO^+. However, at these elevated NO_2 pressures, NO^+ immediately interacts with NO_2 and forms the NO^+NO_2 adducts.

In the reverse experiment, the zeolite samples were first saturated with NO_2 and the weakly adsorbed species were removed by evacuation at room temperature (see Figure 2). Then H_2O was adsorbed onto the thus prepared samples and IR spectra were recorded as the amount of H_2O dosed was increased. The results of these experiments are shown in Figures 7 and 8 for Na− and Ba−Y, respectively. As we have mentioned previously, only NO^+ and nitrate species are present on dry Na−Y zeolite after NO_2 adsorption. On the other hand, on the Ba−Y both NO^+ and a NO^+NO_2 adduct are present at room temperature. Addition of water brings about significant changes in the IR spectra of these NO_2-saturated catalysts. After the first small

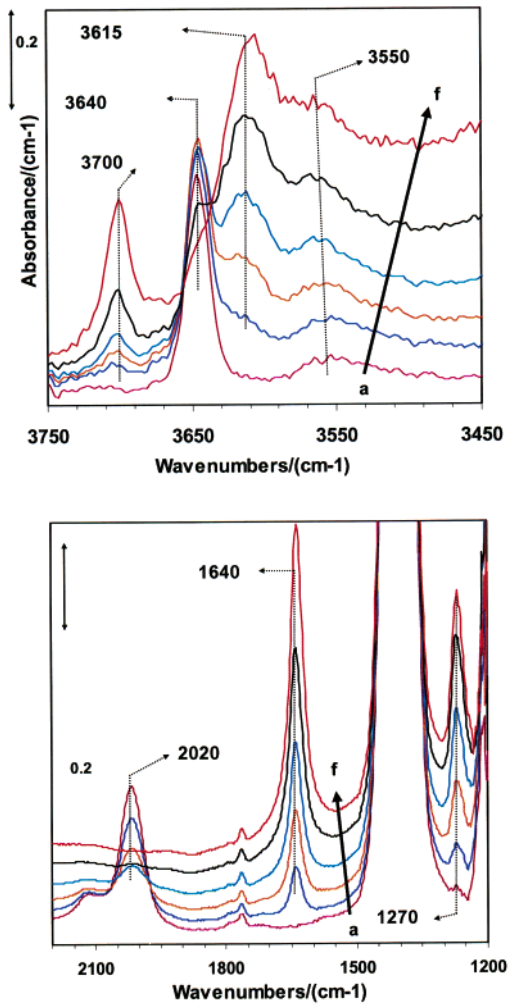

Figure 7. FTIR spectra of water adsorption on $[NO_2]_{ads}$-Na−Y at 295 K. The catalyst was evacuated for 60 min after NO_2 adsorption (a), and then water was dosed (μmol): 1.10 (b), 2.74 (c), 4.63 (d), 7.23 (e), and 10.6 (f).

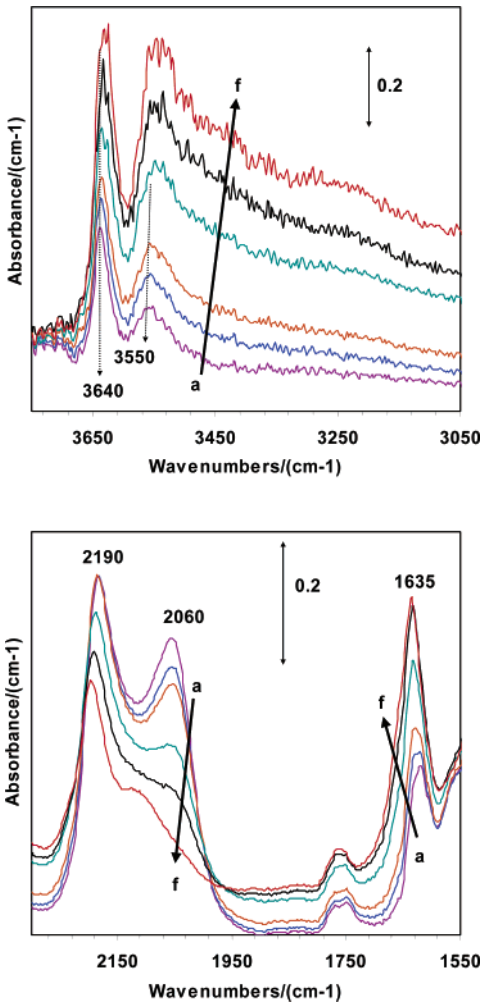

Figure 8. FTIR spectra of water adsorption on $[NO_2]_{ads}$-Ba−Y at 295 K. The catalyst was evacuated for 120 min after NO_2 adsorption (a), and then water was dosed (μmol): 1.08 (b), 1.96 (c), 3.62 (d), 5.50 (e), and 9.65 (f).

water dose, the δ_{HOH} mode of adsorbed water appears at 1640 cm^{-1}, the intensities of the ν_{OH} vibrations of Brønsted acidic OH groups (3640 and 3550 cm^{-1}) increase, the ν_{NO} of NO_2^- (1270 cm^{-1}) develops, while the intensities of the NO^+ features (2020 and 2114 cm^{-1}) decrease. With the increase in the amount of water dosed, the features of adsorbed H_2O and NO_2^- increase gradually, while those of NO^+ decrease and ultimately completely disappear at the highest water dose applied. Similar trends are seen for water adsorption on the NO_2 saturated Ba−Y sample displayed in Figure 8. The intensity of the IR band of adsorbed NO^+ species (2053 cm^{-1}) decreases as water is added to the system and disappears at higher water dosages. Strikingly, there is no change in the intensity of the IR band we have assigned to the NO^+NO_2 adduct. This is somewhat surprising, since this is the species that is removed first upon annealing the NO_2-saturated sample. This observation can be rationalized by assuming that the NO_2 in the NO^+NO_2 adduct interacts fairly strongly with NO^+ thus protecting it from the reaction with water. On the other hand, NO^+ species (just like in the Na−Y case) are susceptible to an attack by the incoming water molecules and this reaction can form HONO and acid sites:

$$2H_2O + -O^-....NO^+ \leftrightarrow -O^-....H_3O^+ + HONO \quad (5)$$

The effect of water on the NO_2 TPD in Na− and Ba−Y is shown in Figure 9. The activated (dry) zeolite samples were contacted with a certain amount of water, then NO_2 was added to the "wet" samples, followed by evacuation and finally TPD. The amount of water added was varied, while that of NO_2 was kept constant at a level that is sufficient for full saturation determined from adsorption experiments. Preadsorbed water significantly altered the NO_2 desorption profiles on both catalysts studied. Over Na−Y (panel A), a high-temperature desorption peak appeared at 520 K in the NO_2 TPD spectrum when the sample was preexposed to a small amount of water prior to saturation NO_2 adsorption. At the same time, the low-temperature desorption feature lost some of its intensity. Increasing the amount of water added onto the activated sample, but keeping the NO_2 dose constant, results in the increase of the high-temperature desorption peak intensity and the decrease in the low-temperature one. There is an interconversion between these two desorption features, that is, as the intensity of the low-temperature desorption feature decreases, that of the high-temperature one increases. At the highest water dose studied, the intensity of the high-temperature desorption feature is higher than that of the low-temperature one. These changes in the NO_2 TPD profile of Na−Y as a consequence of water preadsorption correlate well with the results of the FTIR experiments. These results underscore the relationship between the 2020 cm^{-1} IR feature and the NO_2 desorption feature at 352 K. On the dry Na−Y at room temperature, only the IR absorption features of adsorbed NO^+ and NO_3^- are seen on the evacuted, NO_2-

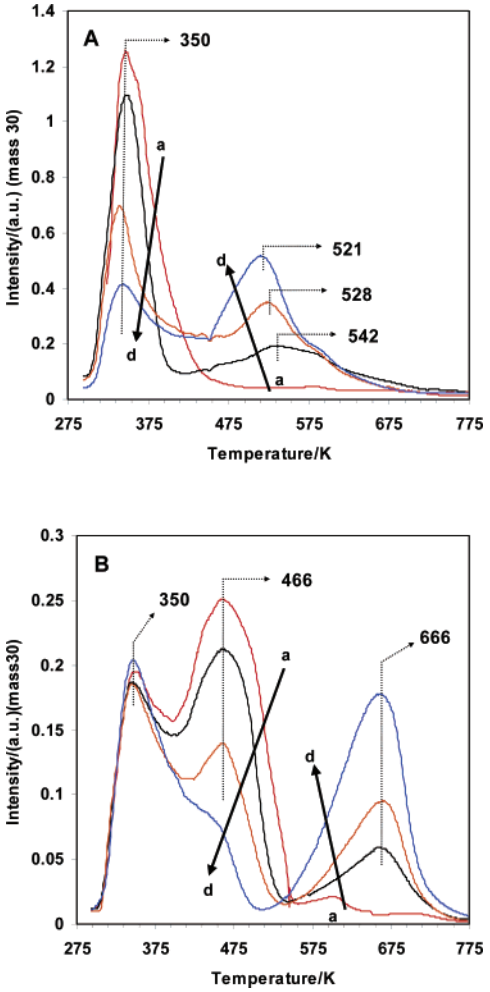

Figure 9. The effect of water on the TPD spectra of adsorbed NO_2 on Na− (A) and Ba−Y (B). The catalysts were first exposed to H_2O and then saturated with NO_2· H_2O doses (μmol): 0 (a), 90.6 (b), 227 (c), and 907 (d) (Weight of catalyst: 0.025 g; heating rate: 5 K/min.)

saturated sample. These species, formed through reaction **1**, can recombine and desorb as NO_2 upon heating the sample, resulting in the disappearance of the 2020 cm^{-1} IR band and the evolution of the TPD feature at 352 K. On the other hand, when water is added either prior to or following NO_2 adsorption, the 2020 cm^{-1} IR feature of adsorbed NO^+ is absent and only the signatures of NO_3^- and NO_2^- are present. These species are stable on the wet Na−Y sample, and upon heating they desorb as NO_2 at a higher temperature of ∼505 K. The high-temperature NO_2 desoprtion peak is always accompanied by the desorption of water (not shown here), which strongly suggests that NO_2 is formed in the reverse of reaction **4**.

The effect of water on the NO_2 TPD of Ba−Y is shown in panel B of Figure 9. The high-temperature (∼470 K) desorption feature shifts upward to ∼660 K. Strikingly, both the intensity and the position of the low-temperature desorption peak stay practically unchanged. Similarly to the Na−Y case, the interconversion between the two high-temperature NO_2 desorption features, as a result of adsorbed water, is apparent over Ba−Y. At the highest water dose studied, the high-temperature NO_2 desorption feature of dry Ba−Y is completely absent, while the 660 K desorption peak reaches its maximum intensity. Correlating the IR and TPD results again helps to explain the observed changes brought about by the coexistence of H_2O and NO_2 on Ba−Y. Water addition onto the NO_2-saturated Ba−Y sample selectively eliminated the 2050 cm^{-1} IR band assigned to adsorbed NO^+. Meanwhile, the NO^+NO_2 adduct was unaffected by preadsorbed H_2O. This somewhat surprising result can be explained by the high reactivity of the NO^+ species. As water is added to the Ba−Y sample containing both NO^+ and NO^+NO_2 adducts, it can react with NO^+ preferentially (and as it turns out exclusively) resulting in the decrease and the ultimate disappearance of the 2050 cm^{-1} IR absorption feature. The NO^+ in the NO^+NO_2 adduct seems to be protected from reacting with water by its strong interaction with NO_2. As we have shown previously, NO^+NO_2 adduct is much more stable over Ba−Y than on Na−Y. Simple room-temperature evacuation completely eliminates the IR feature of NO^+NO_2 on Na−Y, while on Ba−Y this adduct decomposes at around 350 K. This high stability of the NO^+NO_2 adduct in Ba−Y is the reason for the lack of change observed in both the 2185 cm^{-1} IR band and the low-temperature NO_2 TPD feature.

The results presented here may help in understanding the significantly different catalytic activities of Na− and Ba−Y zeolites in the nonthermal plasma assisted selective catalytic reduction of NO_x. Under dry conditions, NO^+ forms in both catalysts; however, its stability in the two materials is vastly different. The much higher stability of NO^+ in Ba−Y translates to a higher concentration of this species at the temperature that the catalytic reaction of interest is run (∼475 K). Because we suspect that this species is an important one in the overall NO_x reduction process, its presence in appreciable concentrations is desirable. Under practical conditions, however, water is always present in the exhaust gas mixture, significantly affecting both the nature and the concentration of adsorbed species present on the surface of the working catalyst. At 475 K operating temperature under these high humidity conditions, zeolites contain appreciable amount of water in their channels. Just approaching it from the NO_2 adsorption standpoint, we showed how significantly water affected both the nature and the quantity of adsorbed NO_x species. In Na−Y, water readily reduces the number of NO^+ species even at room temperature. The quantity of NO^+ species is also decreased by the presence of water in Ba−Y, but some NO^+NO_2 species can form even in the presence of water and may play a role in the observed high activity of Ba−Y.

Here, we only discussed the effect of water on the NO_x adsorption over these catalysts. However, its influence on the adsorption and reactivity of other compounds present in the exhaust gas mixture (in particular partially oxidized hydrocarbons) is unquestionable. In fact, there are indications that water is advantageous in the catalytic process because of its role in suppressing the condensation reaction of acetaldehyde that could eventually lead to catalyst deactivation.[20]

Conclusions

The interaction of NO_2 with both Na− and Ba−Y, FAU zeolites resulted in the formation of the same type of ionic species. In the absence of adsorbed water, NO^+ ions formed by the disproportionation of NO_2 are adsorbed onto framework O^- sites associated with the charge-compensating cationic positions of the zeolite, while NO_3^- ions are bound to the charge-compensating cations. At high NO_2 dosages, NO^+NO_2 adducts can form on both catalysts. The thermal stabilities of these adsorbed NO_x species strongly depend on the nature of the charge-compensating cation. The adsorption of these species is much weaker over Na−Y as a large fraction of the NO^+ and NO_3^- desorb even upon evacuation at 295 K. On the other hand, all the adsorbed NO_x species are much more stable over Ba−Y, so much so, that even most of the NO^+NO_2 species are

present on this catalyst following room temperature evacuation. The presence of water dramatically influences the adsorption of NO_2 on both materials, as it competes for the available adsorption sites and also reacts with some of the adsorbed NO_x species. The number of adsorbed NO^+ species decrease with increasing amount of H_2O added, and HNO_x species are formed that by interacting with the charge-compensating cations form zeolitic $-O-H$ groups and $M^{n+}(NO_x)_n$. The NO_2 TPD feature in $Na-Y$ shifts from 350 to 520 K, while on $Ba-Y$ the corresponding TPD feature shifts from 470 to 670 K. The large differences presented here for the stabilities of adsorbed NO_x species over these two catalysts seem to strongly correlate with their vastly different catalytic activities observed in the non-thermal plasma assisted NO_x reduction.

Acknowledgment. The authors gratefully acknowledge the U.S. Department of Energy (DOE), Office of Energy Efficiency and Renewable Energy, FreedomCAR, and Vehicle Technologies for support of this program. The work was performed as part of a CRADA with the USCAR Low Emissions Technologies Research and Development Partnership (LEP), Pacific Northwest National Laboratory (PNNL), and DOE/OFCVT. The research described in this paper was performed at the Environmental Molecular Sciences Laboratory, a national scientific user facility sponsored by the DOE Office of Biological and Environmental Research and located at the Pacific Northwest National Laboratory (PNNL). PNNL is operated for the U.S. DOE by Battelle Memorial Institute under Contract No. DE-AC0676RLO1831.

References and Notes

(1) Johnson, T. V. **SAE 2002−01−0285**, and references therein.
(2) Hoard, J.; Balmer, M. L. **SAE 982429**.
(3) Hammer, T.; Broer, S. **SAE 982428**.
(4) Balmer, M. L.; Tonkyn, R. G.; Kim, A.; Yoon, S.; Jimenez, D.; Orlando, T.; Barlow, S. E.; Hoard, J. **SAE 982511**.
(5) Fisher, G. B.; DiMaggio, C. L.; Sommers, J. W. **SAE 1999−01−3685**.
(6) Chun, B.-H.; Lee, H.-S.; Nam, C.-S.; Chun, K. M.; Ryu, J. H.; Lee, K.-Y. **SAE 2000−01−2897**.
(7) Fisher, G. B.; DiMaggio, C. L.; Yezerets, A.; Kung, M. C.; Kung, H. H.; Baskaran, S.; Frye, J. G.; Smith, M. R.; Herling, D. R.; LeBarge, W. J.; Krupe, J. **SAE 2000−01−2965**.
(8) Aardahl, C. L.; Habeger, C. F.; Balmer, M. L.; Tran, D. N.; Avila, M.; Park, P. W.; Koshkarian, K. A.; Chanda, A. **SAE 2000−01−2961**.
(9) Tonkyn, R. G.; Yoon, S.; Barlow, S. E.; Panov, A. G.; Kolwaite, A.; Balmer, M. L. **SAE 2000−01−2896**.
(10) Penetrante, B. M.; Brusasco, R. M.; Merritt, B. T.; Pitz, W. J.; Vogtlin, G. E.; Kung, M. C.; Kung, H. H.; Wan, C. Z.; Voss, K. E. **SAE 982508**.
(11) Rappe, K. G.; Aardahl, C. L.; Habeger, C. F.; Tran, D. N.; Delgado, M. A.; Wang, L.-Q.; Park, P. W.; Balmer, M. L. **SAE 2001−01−3570**.
(12) Yoon, S.; Panov, A. G.; Tonkyn, R. G.; Ebeling, A. C.; Barlow, S. E.; Balmer, M. L. *Catal. Today* **2002**, *72*, 243.
(13) Tonkyn, R. G.; Barlow, S. E.; Hoard, J. W. *Appl. Catal., B* **2003**, *40*, 207.
(14) Kwak, J. H.; Szanyi, J.; Peden, C. H. F. *J. Catal.* **2003**, *220*, 291.
(15) Kwak, J. H.; Szanyi, J.; Peden, C. H. F. *Catal. Today* **2004**, *89*, 135.
(16) Szanyi, J.; Kwak, J. H.; Moline, R. A.; Peden, C. H. F. *PCCP* **2003**, *5* (18), 4045.
(17) Hadjiivanov, K. I. *Catal. Rev.—Sci. Eng. 42* (1&2), 71−144 (000).
(18) Ward, J. W. *J. Phys. Chem.* **1968**, *72* (12) 4211.
(19) Sun, Q.; Gao, Z.-X.; Chen, H.-Y.; Sachtler, W. M. H. *J. Catal.* **2001**, *201*, 89.
(20) Wen, B.; Yeom, Y. H.; Weitz, E.; Sachtler, W. M. H., submitted.